

¹ MeMC: A package for monte-carlo simulations of spherical shells

³ **Vipin Agrawal^{1,2}, Vikash Pandey¹, Hanna Kylhammar³, Apurba Dev^{4,5},**
⁴ **and Dhrubadity Mitra¹**

⁵ **1** Nordita, KTH Royal Institute of Technology and Stockholm University, Roslagstullsbacken 23,
⁶ 10691 Stockholm, Sweden. **2** Department of Physics, Stockholm university, Stockholm, Sweden. **3**
⁷ KTH Royal Institute of Technology, Sweden. **4** Department of Electrical Engineering, The Angstrom
⁸ Laboratory, Uppsala University, Uppsala, Sweden. **5** Department of Applied Physics, School of
⁹ Engineering Sciences, KTH Royal Institute of Technology, Stockholm, Sweden.

DOI: [10.xxxxxx/draft](https://doi.org/10.xxxxxx/draft)

Software

- [Review ↗](#)
- [Repository ↗](#)
- [Archive ↗](#)

Editor: [Frederick Boehm ↗](#)

Reviewers:

- [@victorapm](#)
- [@mgiardino](#)

Submitted: 31 March 2022

Published: unpublished

License

Authors of papers retain
copyright and release the work
under a Creative Commons
Attribution 4.0 International
License ([CC BY 4.0](#)).

¹⁰ Summary

¹¹ The MeMC is an open-source software package for monte-carlo simulation of elastic shells. It
¹² is designed as a tool to interpret the force-distance data generated by indentation of biological
¹³ nano-vesicles by atomic force microscopes. The code is written in c++ and python. The code
¹⁴ is customizable – new modules can be added in a straightforward manner.

¹⁵ Statement of need and purpose of software

¹⁶ Micro and nano vesicles, both natural and synthetic, play a crucial role in biology and
¹⁷ medicine. The physical properties of these vesicles play an important role in their biological
¹⁸ functions ([Phillips et al., 2012](#)). Hence it is important to be able to measure their elastic
¹⁹ constants, in particular the Young's modulus and the bending rigidity. One way to measure
²⁰ the elastic constants of biological objects, e.g., a red blood cell (RBC), is to poke them with
²¹ an atomic force microscope (AFM) to obtain a force-distance curve. Then we must model
²² the biological object as an elastic material and by fitting this model to the experimental
²³ force-distance curve estimate the parameters of the elastic model, i.e., the elastic constants.
²⁴ As an example, consider a force-distance curve obtained by AFM measurement of a RBC. The
²⁵ RBC is modeled as a linear elastic material with a Young's modulus, Y_{3d} . Typically a Hertzian
²⁶ model of elastic bodies in contact ([Landau & Lifshitz, 1970, sec. 9](#)) is used to measure Y_{3d} .
²⁷ Nano vesicles differ from (micro-meter scale) cells in two important ways

- ²⁸ 1. The nano-vesicles are much smaller hence thermal fluctuations may effectively renormalize
²⁹ the elastic coefficients ([Košmrlj & Nelson, 2017 ; Paulose et al., 2012](#)).
- ³⁰ 2. Cell membranes are strongly coupled to an underlying cytoskelton. Hence they may be
³¹ modeled by a solid body ([HW et al., 2002](#)) but nano-vesicles must be modeled as liquid
³² filled elastic membranes.

³³ Hence, to be able to interpret the force-distance curve of nano-vesicles, we need to solve for
³⁴ the elastic response of a thermally fluctuating elastic shell.

³⁵ There are commercial packages, e.g., COMSOL ([n.d.-a](#)), to calculate the force-distance curve
³⁶ of solid bodies and closed membranes with fluids inside under the action of external forces but
³⁷ to the best of our knowledge there is no package that includes thermal effects. Monte-carlo
³⁸ simulations of elastic membranes, that does include thermal fluctuations, have been done for
³⁹ more than three decades ([Auth & Gompper, 2005; Bowick et al., 2001; Goetz et al., 1999;](#)
⁴⁰ [Paulose et al., 2012](#)), see also ([Gompper & Kroll, 2004](#) for a review). But to the best of our

⁴¹ knowledge there are no open-source code available. The goal of this package is to fill this gap
⁴² in open-source software.

⁴³ Theoretical background

⁴⁴ Our model of nano-vesicles is an amorphous membrane enclosing an incompressible fluid([Vorselen et al., 2017](#)). Unlike a solid ball, the force-distance relationship for such a model is linear for
⁴⁵ small deformation ([Paulose et al., 2012; Vorselen et al., 2017](#)) if we ignore thermal fluctuations.
⁴⁶ Ref. ([Vorselen et al., 2017](#)) uses a similar model, ignoring thermal fluctuations, to interpret
⁴⁷ AFM measurement of nano-vesicles.

⁴⁹ Let us consider a (three dimensional) material with Young's modulus Y_{3d} and Poisson's ratio
⁵⁰ σ_{3d} and make a membrane out of it. Then the bending modulus and the in-plane Young's
⁵¹ modulus is given by ([Landau & Lifshitz, 1970, sec. 13 and 14](#))

$$B = \frac{Y_{3d}h^3}{12(1 - \sigma_{3d}^2)} \quad \text{and} \quad Y = Y_{3d}h, \quad (1)$$

⁵² where h is the thickness of the membrane. This need not necessarily hold for biological
⁵³ membranes. Nevertheless consider a fluid enclosed in a solid membrane, as done in ([Paulose
⁵⁴ et al., 2012](#)). We consider an elastic energy

$$\mathcal{E}[w, \mathbf{u}] = \int d^2x \left[\frac{B}{2} (\nabla^2 w)^2 + \mu u_{ij}^2 + \frac{\lambda}{2} u_{kk}^2 - pw \right] \quad (2)$$

$$u_{ij} = \frac{1}{2} (\partial_i u_j + \partial_j u_i + \partial_i w \partial_j w) - \delta_{ij} \frac{w}{R} \quad (3)$$

⁵⁶ where w is the out-of-plane deformation of the shell, and \mathbf{u} is the in-plane deformation, p is the
⁵⁷ pressure, λ and μ are the two in-plane Lame coefficients and B is the bending modulus. The
⁵⁸ Lame coefficients are related to other elastic constant as follows ([Landau & Lifshitz, 1970](#))

$$K = \lambda + \frac{2}{3}\mu, \quad Y = \frac{9K\mu}{3K + \mu}, \quad \sigma = \frac{1}{2} \frac{3K - 2\mu}{3K + \mu} \quad (4)$$

⁵⁹ Here K is the volume compressibility, Y the Young's modulus, and σ the Poisson ratio.
⁶⁰ If we consider the material to be incompressible, $K \rightarrow \infty$ and $\sigma = 1/2$, then there are two
⁶¹ elastic constant, the bending rigidity B and the Young's modulus Y . Consequently, there are
⁶² two dimensionless numbers, the Föppl-von-Karman number

$$FvK = \frac{YR^2}{B} \quad (5)$$

⁶³ and the Elasto-Thermal number:

$$ET = \frac{k_B T}{B} \sqrt{FvK}, \quad (6)$$

⁶⁴ where R is the radius of the spherical shell.

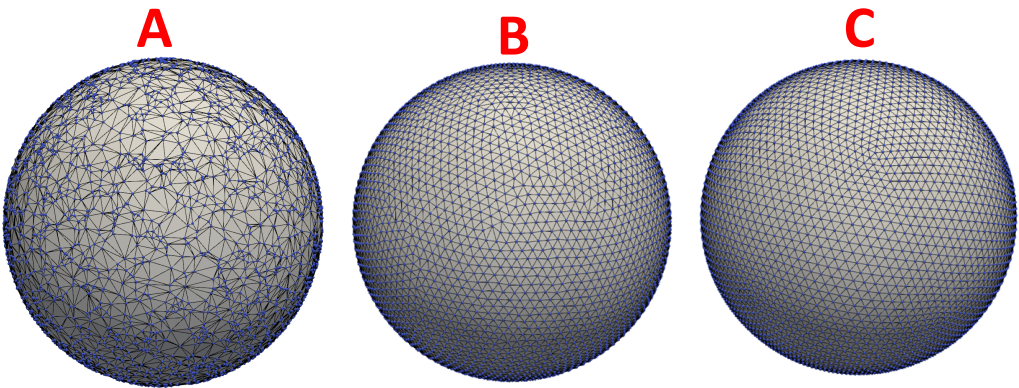
⁶⁵ Using values of Y and B from molecular dynamics simulations of lipid bilayers ([Boek et al.,
⁶⁶ 2005](#)), $Y = 1.7 \text{ N/m}$ and $B = 5k_B T$ and $R = 100$ nano meter, we have $FvK \approx 0.3 \times 10^7$
⁶⁷ which is close to the Föppl-von-Karman number for Graphene sheets and $ET \approx 10^3$.

68 Numerical implementation

69 Grid

70 Following Ref. (Gompper & Kroll, 2004), we use a triangulated-network grid in the following
 71 manner. We start with N randomly chosen points on a sphere. Then, we run a Monte-
 72 Carlo simulation, with a Lennard-Jones (LJ) repelling potential, of these points moving on
 73 the surface. Once the surface Monte-Carlo (SMC) has reached an equilibrium, we use the
 74 algorithm in Ref. (Caroli et al., 2009) to construct the Delaunay triangulation of these points.
 75 The connection between the points thus formed is kept unchanged. In the rest of this paper,
 76 we call this the *initial configuration*(Figure 1(A)). A different snapshot (Figure 1(B)) from the
 77 same equilibrium gives an equivalent but differently triangulated grid.

78 An alternative is to use a regular grid (Buenemann & Lenz, 2008; Vliegenthart & Gompper,
 79 2006). This is achieved by approximating the sphere with geodesic polyhedron (Figure 1(C)).
 80 They are available from the *Meshzoo* library (n.d.-b). In this paper we use $N = 5120$ for the
 81 random grid and $N = 5292$ for the regular grid.



59 **Figure 1: Grid points on a sphere** (A)Triangulated random points on a sphere. (B) Triangulated
 60 points on sphere after 60000 SMC iteration of the initial configuration shown in (A). (C) An example
 61 of regular grid }

62 Energy

63 The basic algorithm of Monte-Carlo simulations is straightforward and well-known (see, e.g.,
 64 Baumgärtner et al., 2013). We randomly choose a point on the grid and move it by a random
 65 amount. We calculate the change in energy due to this movement. We accept or reject
 66 the move by the standard Metropolis algorithm. In our code the energy has the following
 67 contributions

$$E = E_s + E_{\text{bend}} + E_{\text{bulk}} \quad (7)$$

68 where E_s is the contribution from stretching, E_{bend} is the contribution from bending, and
 69 E_{bulk} is the contribution from the bulk modulus. We describe each of these in turn.

70 Stretching

71 In the initial configuration, two neighboring points with coordinates R_i and R_j are connected
 72 by a bond of length ℓ_{ij}^0 . When the i -th point is moved all its bonds with the neighbors change
 73 from their initial length. We model each of these bonds by a harmonic spring and calculate
 74 the stretching energy by

$$E_s = \frac{1}{2} \sum_i \frac{H}{2} \sum_{j(i)} (R_{ij} - \ell_{ij}^0)^2 \quad \text{where} \quad (8)$$

$$\mathbf{R}_{ij} \equiv |\mathbf{R}_i - \mathbf{R}_j|.$$

Here the notation $j(i)$ denotes that the sum is over all the nearest neighbors of the i -the point.

The Láme coefficients and the Young's modulus are given by ([Seung & Nelson, 1988](#))

$$\lambda = \mu = \frac{\sqrt{3}}{4} H, \quad Y = \frac{2}{\sqrt{3}} H \quad (9)$$

98 Bending

An example of triangulated mesh at the node i . α_{ij}, β_{ij} are the angles opposite to the bond ij . Shaded part is the Voronoi region of triangle T defined by nodes $(i, j-1, j)$. Here, we consider that the triangle T is acute.

To calculate the bending contribution, we need to calculate the curvature. In the continuum limit, $N \rightarrow \infty$, bending energy ([Nelson et al., 2004](#)) is:

$$E_B = \frac{B}{2} \int (\nabla^2 \mathbf{R})^2 dS, \quad (10)$$

where $\nabla^2 \mathbf{R}$ is Laplacian of \mathbf{R} on the surface of the sphere.

A general introduction to discretization of Laplacian on a triangulated mesh is given in Refs. ([Hege & Polthier, 2003](#); [Itzykson, 1986](#)). Laplacian on a 2D manifold embedded in \mathbb{R}^3 is:

$$\mathbf{L}(\mathbf{R}) = 2\kappa(\mathbf{R})\hat{m}(\mathbf{R}), \quad (11)$$

where $\kappa(\mathbf{R})$ is the mean curvature, and $\hat{m}(\mathbf{R})$ is the normal to the surface at \mathbf{R} . Note that, $\hat{m}(\mathbf{R})$ is a local property of a point P with coordinates \mathbf{R} and it is not necessarily the outward normal of the closed surface. In the discrete form ([Hege & Polthier, 2003](#); [Meyer et al., 2003](#)),

$$\mathbf{L}_i = \frac{1}{A_i} \sum_{j(i)} \frac{1}{2} [\cot(\alpha_{ij}) + \cot(\beta_{ij})] \mathbf{R}_{ij} \quad (12)$$

A_i is the area of Voronoi dual cell at the node i , and α_{ij}, β_{ij} are the angles opposite to bond ij as shown in [subsubsection](#). Consider the triangle T in [subsubsection](#) defined by its vertices $(i, j-1, j)$. If T is non-obtuse its circumcenter lies within it, hence so does the Voronoi region. Let A^c be the area of shaded region in [subsubsection](#) given by ([Hege & Polthier, 2003](#); [Meyer et al., 2003](#)),

$$A^c = \frac{1}{8} [R_{ij}^2 \cot(\alpha_{ij}) + R_{ij-1}^2 \cot(\beta_{ij-1})]. \quad (13)$$

If there is an obtuse angle in triangle T , the Voronoi region is not necessarily enclosed by the triangle ([Hege & Polthier, 2003](#)). For such cases, instead of A^c , we use A^b , defined as ([Hege & Polthier, 2003](#); [Meyer et al., 2003](#)):

$$A^b = \left\{ \begin{array}{l} \frac{\text{area}(T)}{2}, \text{angle of } T \text{ at } i \text{ is obtuse} \\ \frac{\text{area}(T)}{4}, \text{any other angle is obtuse} \end{array} \right\}, \quad (14)$$

where $\text{area}(T) = 0.5 |\mathbf{R}_{ij} \times \mathbf{R}_{ij-1}|$ is the area of the triangle T . The area A_i is obtained by summing up the contributions in [subsubsection](#) from all the triangles in, e.g., the contribution from the triangle T is the shaded area. For a closed surface the bending energy must be calculated relative to the spontaneous curvature, i.e., its discretised form is :::

$$E_{\text{bend}} = \frac{B}{2} A_i (\mathbf{L}_i - C\hat{n})^2. \quad (15)$$

122 :: where C is the spontaneous curvature, for a sphere $C = 2/R$, where R is radius of the
 123 sphere and \hat{n} is the outward normal to the surface. Hence not only the magnitude but also
 124 the vector nature of the surface Laplacian must be determined. For every triangle in the
 125 initial configuration, i.e., when all the points lie on the surface of a sphere, the outward unit
 126 normal can be calculated in a straightforward manner. For example, for the triangle T in
 127 [subsubsection](#), it can be calculated by finding out the unit vector that points along $\mathbf{R}_{ij-1} \times \mathbf{R}_{ij}$.
 128 Hence, at any time, if we access the points around the node i in counterclockwise manner
 129 when viewed from outside we are guaranteed to obtain the outward normal. We ensure this
 130 by sorting appropriately the points around every node in the initial configuration. As the
 131 connectivity of the mesh remains unchanged this property is preserved at all future times.
 132 To sort the neighbors around any node i , we rotate the coordinate system such that, the z
 133 axis passes through the point i along the vector \mathbf{R}_i . In this coordinate system we sort the
 134 neighbors by their azimuthal angle. Note that unlike Ref. ([Gompper & Kroll, 2004](#)) we do not
 135 incorporate self-avoidance.

136 **Bulk**

137 We assume that the liquid inside the vesicle is incompressible ¹. This is implemented by adding
 138 a energy cost to the volume change. At any point, the total contribution to the bulk energy is

$$E_{\text{bulk}} = K \left(\frac{V}{V_0} - 1 \right)^2, \quad (16)$$

139 where K is bulk modulus, V is current volume, and V_0 is the initial volume of the vesicle. As
 140 we move the point i by a random amount, the change in bulk energy is

$$\Delta E_{\text{bulk}} = 2K \frac{\Delta V(V - V_0)}{V_0^2} + \left(\frac{\Delta V}{V_0} \right)^2, \quad (17)$$

141 where ΔV is the change in volume due to the move.

142 **Sticking to a solid surface**

143 As a specific example of nano-vesicle, we consider an exosome. We quote from Ref. ([Pegtel &](#)
 144 [Gould, 2019](#)) " Exosomes are small, single-membrane, secreted organelles of ~ 30 to ~ 200 nm
 145 in diameter that have the same topology as the cell and are enriched in selected proteins, lipids,
 146 nucleic acids, and glycoconjugates. " The exosomes that we consider here were collected from
 147 immortalized cell line and extracted following the procedures as described in Ref. ([Cavallaro
 et al., 2019](#)). To measure the force-distance curve it is necessary to fix an exosome on a
 148 transparent coverslip. This was done by electrostatic coupling to a PLL coated surface by
 149 incubating them at room temperature for one hour, see Ref ([Cavallaro et al., 2019](#)). As an
 150 illustration, in [Figure 2](#), we show a typical experimental measurement of the height above a
 151 flat surface as measured by the AFM. After being stuck to the flat surface the free surface
 152 forms a spherical cap. To reproduce such experiments as closely as possibly we need to fix the
 153 vesicle to a flat surface. This is implemented by the Lennard-Jones potential:

$$V_{\text{LJ}}(r) \equiv 4\epsilon_w \left[\left(\frac{\sigma_w}{r} \right)^{12} - \left(\frac{\sigma_w}{r} \right)^6 \right] \quad (18)$$

155 What fraction of the vesicle is fixed to the flat surface is parametrized by the angle Θ_0 (see
 156 [Figure 2\(B\)](#)) which is a parameter in our code. We choose a system of coordinates with its
 157 origin at the center of the vesicle and the z axis pointing radially outward through the north
 158 pole. All the grid points on the surface whose polar angle is greater than Θ_0 are selected such
 159 that the sticking potential acts only on them, see [Figure 2\(B\)](#).

¹This is different from assuming a semi-permeable membrane, as done in Ref. ([Vorselen et al., 2017](#)), in which case the liquid can flow in or out and the osmotic pressure of solutes decreases and increases accordingly.

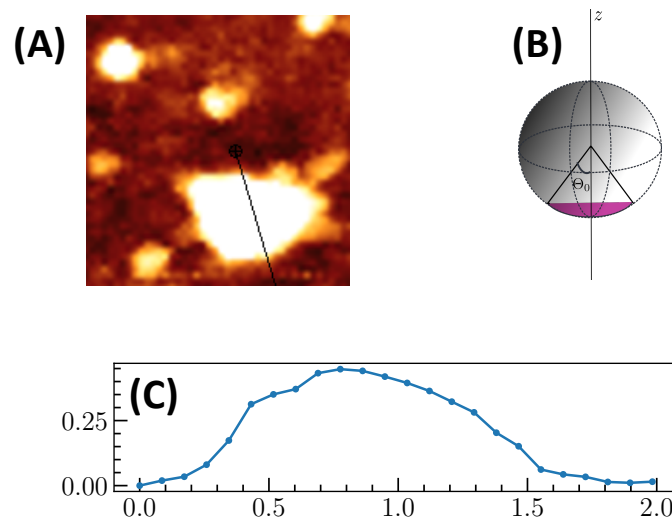


Figure 2: (A) A colormap of the height as measured by the AFM. (B) Illustration of the vesicle stuck to a surface by an angle Θ_0 . (C) The height plotted along the line shown in (A).

160 AFM tip

161 To model the interaction between AFM tip and the vesicle, We model the shape of tip as
 162 paraboloid and we use only the repelling part of the Lennard-Jones potential:

$$V_{RLJ}(r) \equiv 4\epsilon_A \left(\frac{\sigma_A}{r} \right)^{12} \quad (19)$$

163 For every point on the vesicle, we calculate the shortest distance of this point to the paraboloid
 164 and use this distance as the argument of function V_{RLJ} in [Equation 19](#).

165 Dependencies

166 The code requires the following:

- 167 ▪ A c++ compiler. We have tested the code against gnu g++ version 11.2.0 on x86_64
 168 CPU.
- 169 ▪ Hdf5 libraries for reading and writing data.
- 170 ▪ Python version 3.8 with scipy, numpy, h5py and numpy-quaternion installed.
- 171 ▪ For three-dimensional visualization we use VisIt ([Childs et al., 2012](#)).

172 Typical workflow and test

173 We have tested our code in LINUX operating system. We expect it to work without any
 174 problem in any similar environment. It may also work with WINDOWS although we have not
 175 tested this aspect.

176 The github repository ([n.d.-c](#)) contains a file named README.md that contains instruction to
 177 install and run the code. In [Figure 3](#) we show three typical snapshots from our code for three
 178 different position of the AFM tip.

179 In the github repository, we also provide a subdirectory called Examples. By executing the
 180 shell script execute.sh in that directory the user can run the code (without the AFM tip and

181 the bottom plate). It takes almost 30 minutes on Intel(R) Core(TM) i5-8265U CPU. The run
 182 produces a probability distribution function (PDF) of the total energy after 50,000 number
 183 of monte-carlo steps. By running `gnuplot plot.gnu` (this requires the software gnuplot) the
 184 user can compare the PDF obtained by their run with a PDF that we provide.

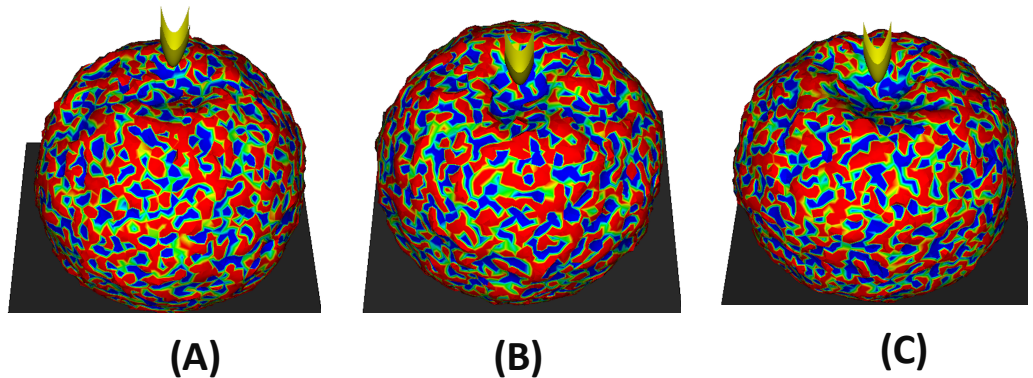


Figure 3: Representative snapshots from our code for three different positions (tz) of the AFM tip. The origin of our coordinate system is at the center of the undeformed sphere and the radius of the undeformed sphere is unity. The colormap shows the signed curvature (Equation 11; red(positive) and blue(negative)). (A) $tz = 1.05$, (B) $tz = 0.9$, (C) $tz = 0.75$

185 We acknowledge the support of the Swedish Research Council Grant No. 638-2013-9243 and
 186 2016-05225. The simulations were performed on resources provided by the Swedish National
 187 Infrastructure for Computing (SNIC) at PDC center for high performance computing.

188 References

- 189 (n.d.-b). <https://github.com/meshpro/meshzoo>.
- 190 (n.d.-c). <https://github.com/vipinagrawal25/MeMC>.
- 191 (n.d.-a). <https://www.comsol.com>.
- 192 Auth, T., & Gompper, G. (2005). Fluctuation spectrum of membranes with anchored linear
 193 and star polymers. *Physical Review E*, 72(3), 031904.
- 194 Baumgärtner, A., Binder, K., Hansen, J.-P., Kalos, M., Kehr, K., Landau, D., Levesque, D.,
 195 Müller-Krumbhaar, H., Rebbi, C., Saito, Y., & others. (2013). *Applications of the monte
 196 carlo method in statistical physics* (Vol. 36). Springer Science & Business Media.
- 197 Boek, E., Padding, J., Otter, W. K. den, & Briels, W. J. (2005). Mechanical properties
 198 of surfactant bilayer membranes from atomistic and coarse-grained molecular dynamics
 199 simulations. *The Journal of Physical Chemistry B*, 109(42), 19851–19858.
- 200 Bowick, M. J., Cacciuto, A., Thorleifsson, G., & Travesset, A. (2001). Universality classes
 201 of self-avoiding fixed-connectivity membranes. *The European Physical Journal E*, 5(2),
 202 149–160.
- 203 Buenemann, M., & Lenz, P. (2008). Elastic properties and mechanical stability of chiral and
 204 filled viral capsids. *Physical Review E*, 78(5), 051924.
- 205 Caroli, M., Castro, P. M. M. de, Loriot, S., Rouiller, O., Teillaud, M., & Wormser, C. (2009).
 206 *Robust and efficient delaunay triangulations of points on or close to a sphere* [PhD thesis].
 207 INRIA.

- 208 Cavallaro, S., Horak, J., Hågg, P., Gupta, D., Stiller, C., Sahu, S. S., Gorgens, A., Gatty, H.
209 K., Viktorsson, K., El Andaloussi, S., & others. (2019). Label-free surface protein profiling
210 of extracellular vesicles by an electrokinetic sensor. *ACS Sensors*, 4(5), 1399–1408.
- 211 Childs, H., Brugger, E., Whitlock, B., Meredith, J., Ahern, S., Pugmire, D., Biagis, K., Miller,
212 M., Harrison, C., Weber, G. H., Krishnan, H., Fogal, T., Sanderson, A., Garth, C., Bethel,
213 E. W., Camp, D., Rübel, O., Durant, M., Favre, J. M., & Navrátil, P. (2012). VisIt:
214 An End-User Tool For Visualizing and Analyzing Very Large Data. In *High Performance
215 Visualization—Enabling Extreme-Scale Scientific Insight* (pp. 357–372).
- 216 Goetz, R., Gompper, G., & Lipowsky, R. (1999). Mobility and elasticity of self-assembled
217 membranes. *Physical Review Letters*, 82(1), 221.
- 218 Gompper, G., & Kroll, D. (2004). Triangulated-surface models of fluctuating membranes.
219 In D. Nelson, T. Piran, & S. Weinberg (Eds.), *Statistical mechanics of membranes and
220 surfaces* (pp. 359–426). World Scientific.
- 221 Hege, H.-C., & Polthier, K. (2003). *Visualization and mathematics III*. Springer Science &
222 Business Media.
- 223 HW, G. L., Wortis, M., & Mukhopadhyay, R. (2002). Stomatocyte–discocyte–echinocyte
224 sequence of the human red blood cell: Evidence for the bilayer–couple hypothesis from mem-
225 brane mechanics. *Proceedings of the National Academy of Sciences*, 99(26), 16766–16769.
- 226 Itzykson, C. (1986). In J. et al Abad (Ed.), *Proceedings of the GIFT seminar, jaca 85* (pp.
227 130–188). World Scientific Singapore.
- 228 Košmrlj, A., & Nelson, D. R. (2017). Statistical mechanics of thin spherical shells. *Physical
229 Review X*, 7(1), 011002.
- 230 Landau, L., & Lifshitz, E. (1970). *Theory of elasticity* (Vol. 7). Pergamon Press Ltd.
- 231 Meyer, M., Desbrun, M., Schröder, P., & Barr, A. H. (2003). Discrete differential-geometry
232 operators for triangulated 2-manifolds. In *Visualization and mathematics III* (pp. 35–57).
233 Springer.
- 234 Nelson, D., Piran, T., & Weinberg, S. (2004). *Statistical mechanics of membranes and
235 surfaces*. World Scientific.
- 236 Paulose, J., Vliegenthart, G. A., Gompper, G., & Nelson, D. R. (2012). Fluctuating shells
237 under pressure. *Proceedings of the National Academy of Sciences*, 109(48), 19551–19556.
- 238 Pegtel, D. M., & Gould, S. J. (2019). Exosomes. *Annual Review of Biochemistry*, 88, 487–514.
- 239 Phillips, R., Kondev, J., Theriot, J., Garcia, H. G., & Orme, N. (2012). *Physical biology of
240 the cell*. Garland Science.
- 241 Seung, H. S., & Nelson, D. R. (1988). Defects in flexible membranes with crystalline order.
242 *Physical Review A*, 38(2), 1005.
- 243 Vliegenthart, G. A., & Gompper, G. (2006). Mechanical deformation of spherical viruses with
244 icosahedral symmetry. *Biophysical Journal*, 91(3), 834–841.
- 245 Vorselen, D., MacKintosh, F. C., Roos, W. H., & Wuite, G. J. (2017). Competition between
246 bending and internal pressure governs the mechanics of fluid nanovesicles. *Acs Nano*, 11(3),
247 2628–2636.